Iraqi Journal of Physics, 2024 *Vol. 22, No. 1, PP. 31-41*

https://doi.org/10.30723/ijp.v22i1.1194 *P-ISSN: 2070-4003*
E-ISSN: 2664-5548

Influence of A.C. Frequency on Hollow Magnetron Sputtering Discharge Parameters

Zahraa Mohammed Hasan [1a*] and Qusay Adnan Abbas[1b]
[1]*Department of Physics, College of Science, University of Baghdad, Baghdad, Iraq*
[b]E-mail: qusay.a@Sc.Uobaghdad.edu.iq
[a*]Corresponding author: zahraa.hasan2204m@sc.uobaghdad.edu.iq

Abstract

In the present work, optical emission spectroscopy was used to diagnose the influence of A.C. power source frequency on the hollow magnetron sputtering discharge parameters (such as discharge emission, discharge current and voltage, glow discharge structure, temperature (T_e) and electron number density (n_e), Debye length (λ_D), and plasma parameter (N_D) of constant pressure. The electron temperature and number density were determined using the Boltzmann plots and the Stark broadening methods, respectively. The results illustrate that the normal glow discharge structure is similar to the D.C. discharge mode. The magnetic field has no impact on the fundamental discharge parameter in both A.C. frequencies under study. On the other hand, the other discharge parameters (T_e, ne, λ_D, and N_D) increase with increasing the magnetic field in both discharge frequencies. In addition, the increase in the frequency of the A.C. source current led to an increase in the discharge intensity emission and the other discharge parameters being studied. In this case, in frequency 7 kHz, T_e surged from 0.685 eV to 0.839-eV, and n_e experienced an increase from 3.088 x 10^{18} m^{-3} to 4.902 x 10^{18} $m^{-}3$. At a frequency of 9 kHz, the electron temperature surged from 0.711eV to 0.911 eV. n_e experienced an increase from 3.615 x 10^{18} m^{-3} to 6.749 x 10^{18} m^{-3}.

Article Info.

Keywords:
Hollow Electrode, Electron Temperature, A.C. Discharge, Electron Number Density, Discharge Current.

Article history:
Received: Aug. 17,2023
Revised: Oct. 19, 2023
Accepted: Nov. 08, 2023
Published: Mar. 03,2024

1. Introduction

Magnetron Sputtering Systems (MSS) are extensively utilized for the deposition of dielectric, metallic, and compound film coatings on the surface of materials due to their high attainable deposition rate, and high quality and diverse functional properties [1]. Magnetron plasma sources are extensively used in various industrial and technological processes, particularly those that include sputter-etching and thin-film deposition [2, 3].

MSS are typically constructed of conductive materials that conduct electromagnetic energy into the reactor. Glow discharge plasma is a partially ionized gas made up of electrons, positive ions, and a significant number of neutral species. It is one way to create plasma at low pressure. It is simple to produce glow-discharge plasma using a high-voltage electrical discharge and a low-pressure gas system. Creating gas discharge plasma in a diode gap under electric and magnetic cross-fields is the foundation of MSS operation. Sputtering magnetrons are used for etching and thin film deposition. Positive ions of energies of a few hundred eV extracted from plasma (generated from the ionization processes between energetic electrons and a low-pressure gas) impact a negatively biased target, ejecting atoms that will be deposited on a specific substrate as a thin film. In magnetron sputtering, a magnetic field is employed to trap electrons close to the target. These trapped electrons will generate ions that are accelerated into the target by the plasma sheath, causing the desired sputtering. This will increase the ionization of the low-pressure gas, thus increasing plasma density, allowing sputtering at lower pressures and voltages [4-6].

A reactive gas, a non-inert gas, such as oxygen and nitrogen, is sometimes

introduced with the argon gas to form the plasma. The sputtered particles from the target material undergo a chemical reaction, so the thin film deposited on the substrate is of different composition [7]. Reactive sputtering is of two types: the D.C. reactive sputtering and the radio-frequency (RF) reactive sputtering. In the D.C. mode, a continuous or pulsed D.C. voltage is supplied to the target [8]. An RF plasma thruster typically consists of an RF antenna, a discharge chamber, and a magnetic circuit [9, 10]. D.C. sputtering is suitable for conductive materials, whereas RF sputtering is suitable for nonconductive materials. The advantage of RF magnetron sputtering is that magnets better ionize the material in the electric and magnetic fields, allowing the material to pass into plasma form. A.C. magnetron sputtering, in which a magnetic field is superimposed on an electric field, is one of the most prevalent sputtering techniques. This confines electrons to the target, resulting in increased ionization of the sputtering gas and, consequently, faster deposition rates [11, 12].

This work aims to study the A.C. discharge in a cylindrical magnetron sputtering device for plasma characterization. A comprehensive experimental study was carried out to verify the general properties of the plasma and measure the plasma coefficient in hollow-cylindrical magnetron.

2. Methodology

The electrons temperature (T_e) is the most significant factor in describing the plasma state. T_e can be calculated using the Boltzmann plot method as follows [13-19]:

$$\mathrm{Ln}\left(\frac{I_{ji}\,\lambda_{ji}}{g_j A_{ji}}\right) = \left(-\frac{E_{k,z}}{K_B T_e}\right) + \ln\left(\frac{hcL_{nz}}{4\pi p_z}\right) \quad (1)$$

where: Z represent the ionization state, h is Planck's constant, c is speed of light, K_B is Boltzmann constant, j is the highest energy level, i is the lower energy level, λ_{ji} is the wavelength corresponding to the transition between level j and level i for the same ionization degree, A_{ji} the transition probability corresponds to transition from j to i, I_{ji} is the intensity of transition from j to i, P_Z is the species partition function in ionization stage Z, and g_j is a statistical weight. The electron temperature was calculated by plotting the left-hand side of Equation (1) in comparison to the species' higher-level energy during the Z ionization phase, expressed in units of eV [20-23].

Using the Stark-Widening relation, the electron number density (n_e), was calculated as follows [24-29]:

$$n_e(\mathrm{cm}^{-3}) = \left[\frac{\Delta\lambda}{2\omega_s(\lambda, Te)}\right] N_r \quad (2)$$

where: $\Delta\lambda$ is the full width at half maximum of the line, and ω_s is the theoretical line full-width Stark broadening parameter, which is calculated at the same reference electron density $10^{16}(\mathrm{cm}^{-3})$ [30-32].

Debye length (λ_D) is calculable using the formula [33-44]:

$$\lambda_D = \left(\frac{\varepsilon_o k_B Te}{e^2 ne}\right)^{\frac{1}{2}} \quad (3)$$

where: k_B denotes Boltzmann constant.

The value of N_D indicates the total number of particles included in Debye's sphere, which is based on how dense the electrons are, e: electron charge in (C) [45]; this is the second condition for plasma to exist [46-51]:

$$N_D = \frac{4\pi}{3} n_e \lambda_D^3 \cong 1.38 \times 10^6 \frac{[T_e(K°)]^{\frac{3}{2}}}{[n_e(m^{-3})]^{\frac{1}{2}}} \quad (4)$$

3. Experimental

The system used in this work is an RF magnetron sputter with an A.C. discharge power source. Fig. 1 illustrates the diagram of the A.C. magnetron sputtering system which was developed and built. It is composed of a cylindrical magnetron with an A.C. discharge for sputtering. This system consists of stainless-steel vacuum chamber, which is evacuated to a base pressure of 0.4 torr to evaluate discharge behavior, two aluminum coaxial cylindrical electrodes, a D.C. magnetic coil, and an A.C. power source. The discharge gas was argon gas (99.998% pure) under a pressure of 0.4 torr. The vacuum chamber consists of an outer cylinder (wall of the chamber), 25 cm in diameter and 22cm in length, which is the grounded electrode, and an inner cylinder, 3 cm in diameter and 18 cm in length, which is the powered electrode. The glow discharge normal mode was generated by applying a continuous potential of around 10 kV between the two coaxial electrodes and discharge currents (0, 2, 4, 6 amps) for 7 and 9 kHz frequencies to produce the A.C. glow discharge in argon gas (99.9% impurity) at 0.4 torr pressure. A D.C. magnetic solenoid of 500 turns, 2 mm inner diameter and length of 22 cm was used to generate a strong magnetic field to confine the plasma in the central region between the two coaxial cylinders .

For the diagnostic, a compact spectrometer (Thorlabs-CCS 100/M) was used with the following specifications: a wavelength range of 320-740 nm, S/N ratio of 2000:1, a CCD sensitivity of 160 V/ (Ix.s), integration time of 10μs –60s and has full width at half maximum (FWHM) spectral accuracy of 0.5 nm at 435 nm. A holder attaches the optical fiber of the spectrometer to the center point between the electrodes, about 6 cm from the inner electrode, using a quartz lens. The plasma properties were determined by

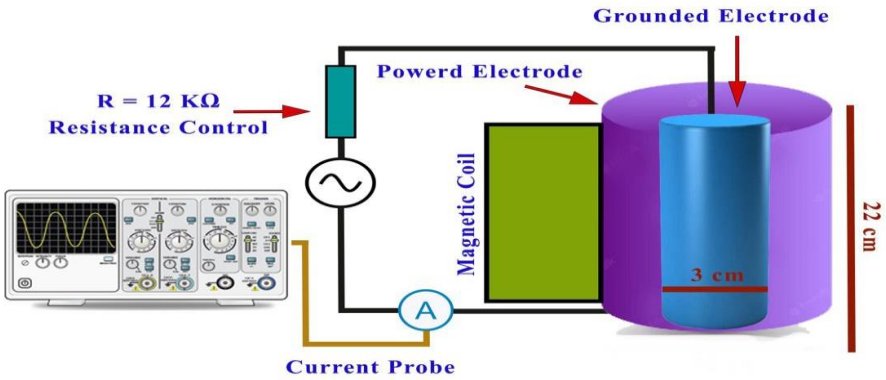

Figure 1: The inverted configuration of the cylindrical magnetron sputtering system.

4. Results and Discussions

4.1. Emission Spectra of Plasma without Magnetic Field

By analyzing the plasma light emissions in the wavelength region of 320–740 nm, using the compact spectrometer (Thorlabs-CCS 100/M), optical emission spectra (OES) were able to identify plasma emissions. Figs. 2 and 3 show the OES of the plasma for different values of the A.C. discharge current at two frequencies. The spectra display five emission peaks of neutral argon (ArIl) at 361.181, 427.752, 434.806, 476.486, and 487.986 nm, in addition to five atomic emission peaks of argon (ArI) located at 419.831, 687.128, 696.543, 706.873, and 738.398 nm. It is clear from these data that the increase in the coil current (0,2,4,6 Amp) led to an increase in the emission peak intensity of all emission peaks (both atomic and ionic peaks) due to an increase in the number of inelastic collisions that took place in the plasma as a result of plasma confinement [13].

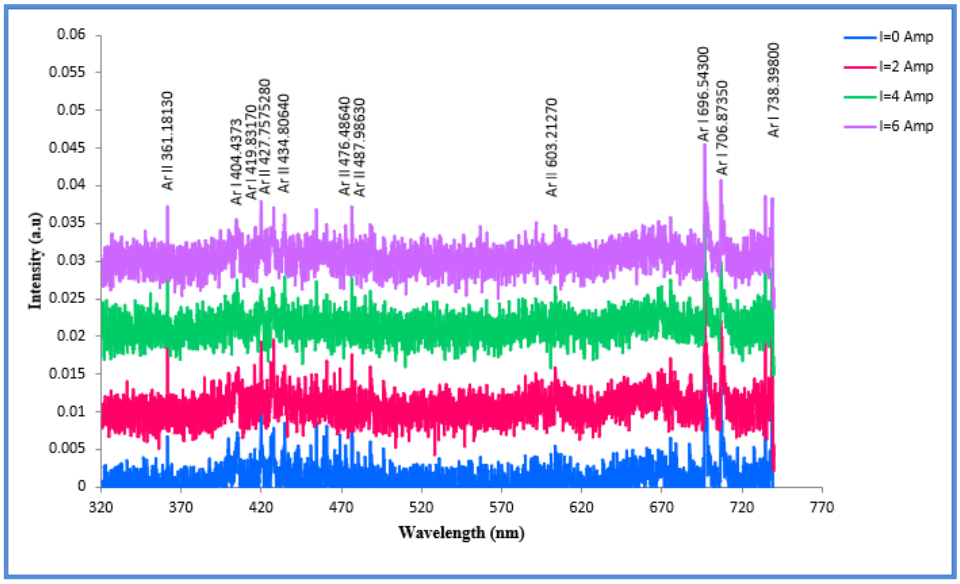

Figure 2: Effect of the coil current on the optical emission spectra of A.C. argon plasma for a frequency of 7 kHz at 0.4 torr.

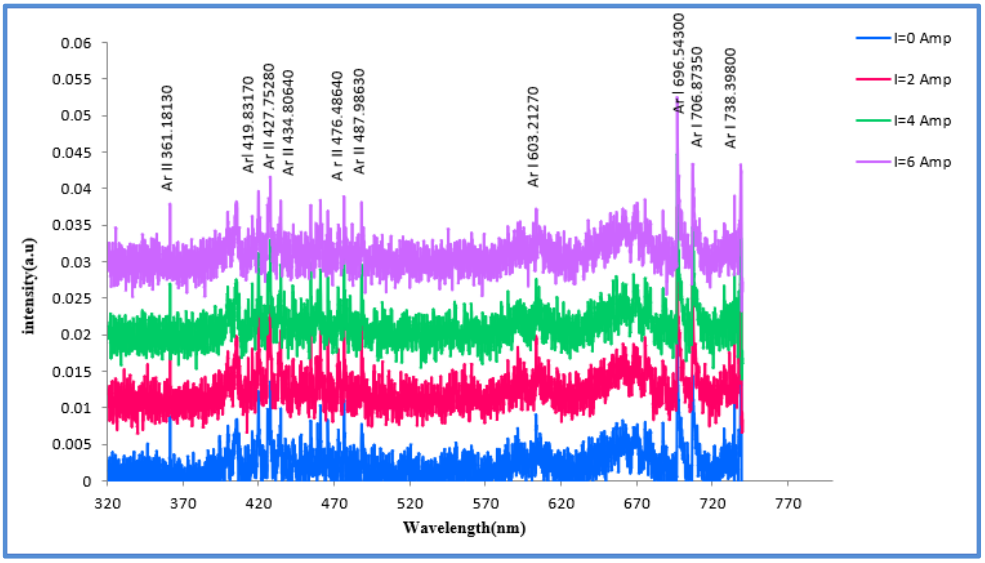

Figure 3: Effect of the coil current on the optical emission spectra of A.C. argon plasma for frequency of 9 kHz at 0.4 torr.

4.2. Influence of Magnetic Field on Normal Glow Discharge Regions

Fig. 4 illustrates how the coil current modifies the typical light regions of a hollow-powered cylinder magnetron device at a constant pressure of 0.4 torr. According to this configuration, the discharge regions within the cylindrical cavity can carry currents on the order of several amperes at a falling voltage of several hundred volts. It features a distribution of varied areas in the hollow-cylindrical discharge mode, as shown in the zones in a circular pattern inside the hollow-powered electrode while gas is forced through a hot, glowing cylinder. The gas will effectively be ionized and heated at the powered zone. From there, plasma flows along the magnetic field to the grounded region, where a significant amount of it recombines. An extremely powerful and uniform plasma is created with the aid of electrostatic and magnetic forces.

Fig. 4 (a, b) show it not has the same effect as increasing the magnetic field (increasing the coil current), which compresses the plasma region and creates a thin layer of luster that confine the plasma. The optical diagnostics applied to a discharge visualize the plasma region corresponding to the confined electrons, represented by the bright area near the target surface observable by the naked eye. This region corresponds to a spatial segment formed by the magnetic lines in the target vicinity.

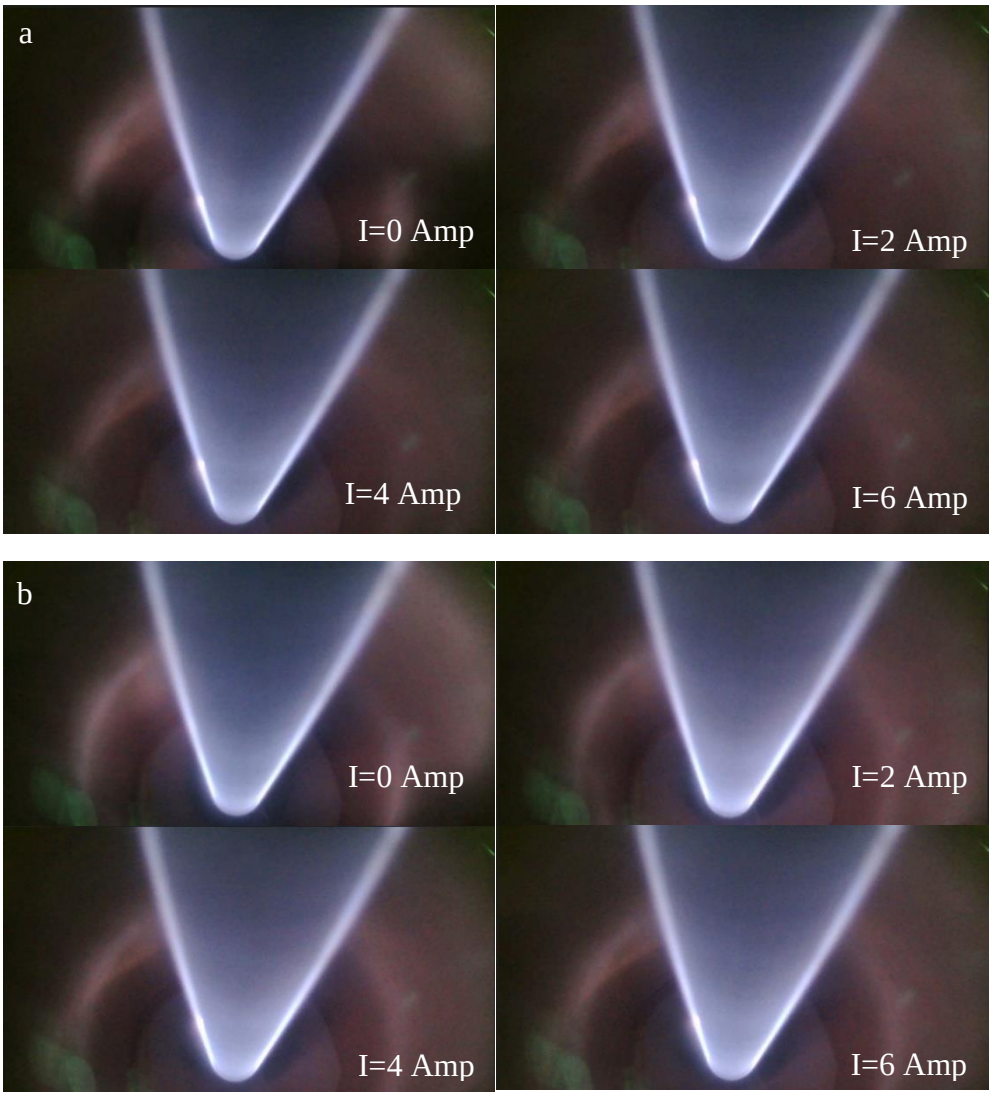

Figure 4: photographs for the A.C. glow discharge structure at a constant pressure of 0.4 torr for different coil currents with frequencies of (a)7 kHz (b)9kHz.

4.3. Fundamental Discharge Characteristic

Fig. 5 shows the effect of the coil current on the discharge voltage at two A.C. source current frequencies. The discharge voltage has approximately a constant value as the coil current increases. The discharge voltage increased when the source current frequency was increased from 7 kHz to 9 kHz. The increase of the discharge voltage with the source current frequency is attributed to the increase of the space charge effect caused by the increase in ionization collisions of electrons with neutral atoms, which causes an increase in the voltage needed to maintain the discharge.

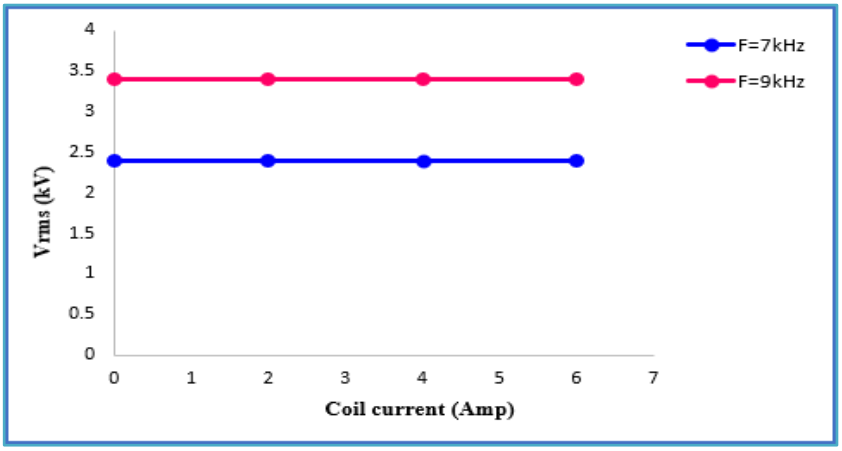

Figure 5: Influence of A.C. source frequency on the change of the voltage discharge with the coil current.

Fig. 6 shows the effect of the A.C. source frequency on the relation between the discharge current and the coil current. At the higher frequency of 9 kHz, the discharge current remains constant as the coil current increases (plasma confinement increases). The increase in plasma confinement means that the ionization collisions of electrons with neutral atoms increase.

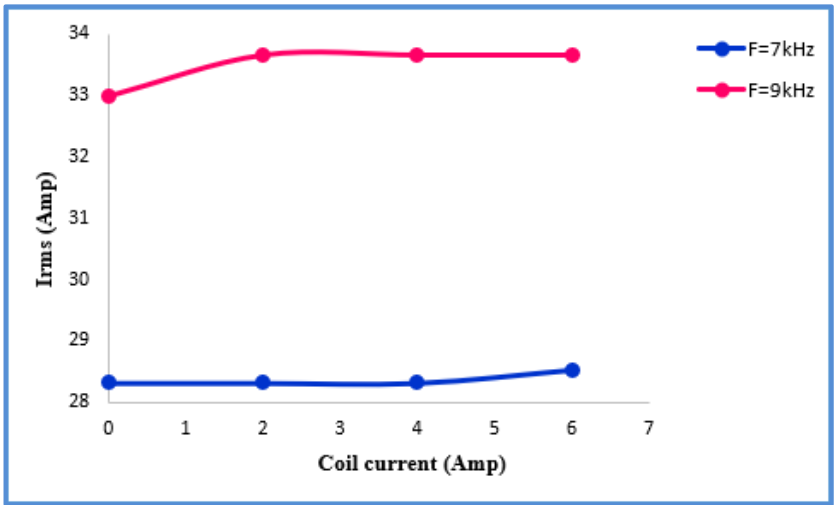

Figure 6: The change of discharge current with the coil current at various A.C. source frequencies.

4.4. Variation of Plasma Particles with Coil Current in Hollow-Cylindrical Magnetron Configuration

T_e is the most important plasma parameter for describing the state of the plasma. It is responsible for regulating a wide range of plasma processes, including ionization and excitation. To compute T_e, assume that the plasma is in thermodynamic equilibrium and that the number of excited atoms follows a Boltzmann distribution. Boltzmann plots were drawn according to Eq. (1) with the data listed in Table 1. The electron temperature can be determined from the slope of the straight line of the Boltzmann plot.

Table 1: Ar II standard lines determine electron temperature and properties [52].

Ion	Ej(eV)	Ei(eV)	Ag(S^{-1})	λ(nm)
Ar II	21.492	18.060	2×10^{6}	361.181
Ar II	21.351	18.454	3.2×10^{8}	427.752
Ar II	19.494	18.643	9.368×10^{8}	434.806
Ar II	19.867	17.265	2.6×10^{8}	476.486
Ar II	19.680	17.140	4.94×10^{8}	487.986

Figs.7 and 8 display the Boltzmann plots for the hollow-discharge configuration employing the specified ionic argon lines (Ar Il) at various coil currents and = 7kHz and 9kHz source frequencies, respectively. The electron temperatures are listed in Table 2.

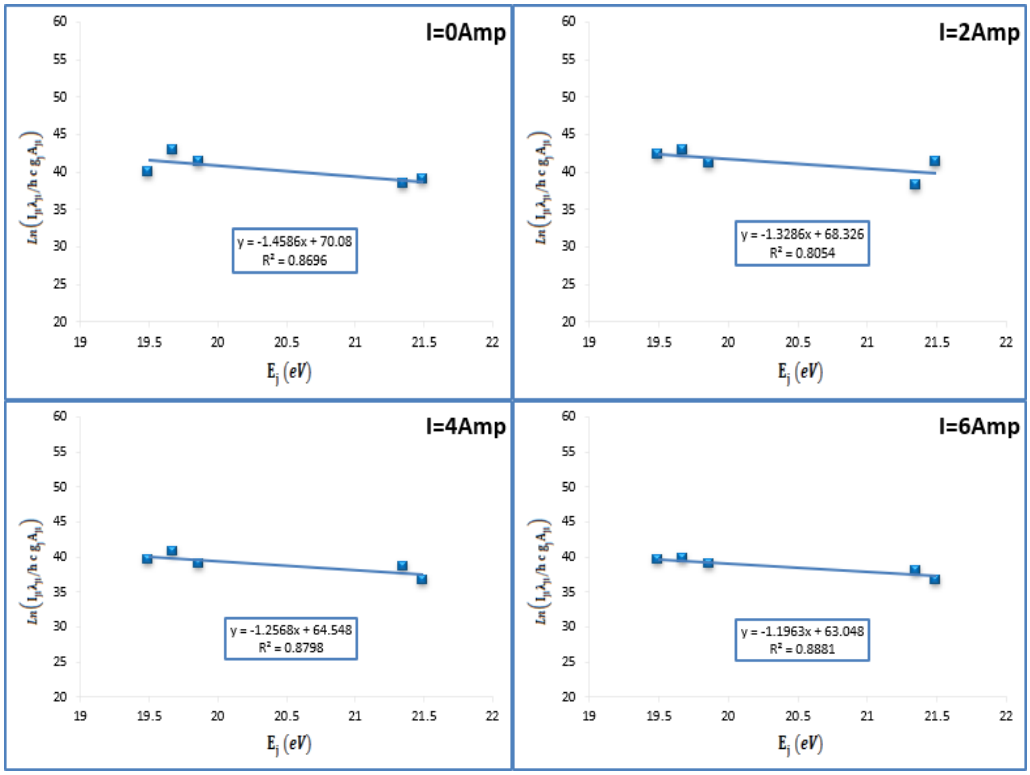

Figure 7: Boltzmann plots for a hollow-discharge configuration with chosen ionic argon lines (Arll) at different coil currents and a source frequency of 7 kHz.

The Stark broadening effect was used to determine n_e, as defined by Equation (2), listed in Table 2. Fig. 9 shows the effect of A.C. source frequency on the change of T_e and n_e as the coil current of the hollow-cylindrical magnetron sputtering device increased. Increasing the coil current causes an increase in the density and temperature of the electrons at the two frequencies. The increases in n_e with increasing coil current may be attributed to the increase of the inelastic collisions of electrons with the argon

atoms caused by magnetic confinement. The magnetic confinement of electrons in the area close to the powered electrode surface, where the electric field is present, may cause an increase in the electron temperature with increasing the coil current (increase of the magnetic field).

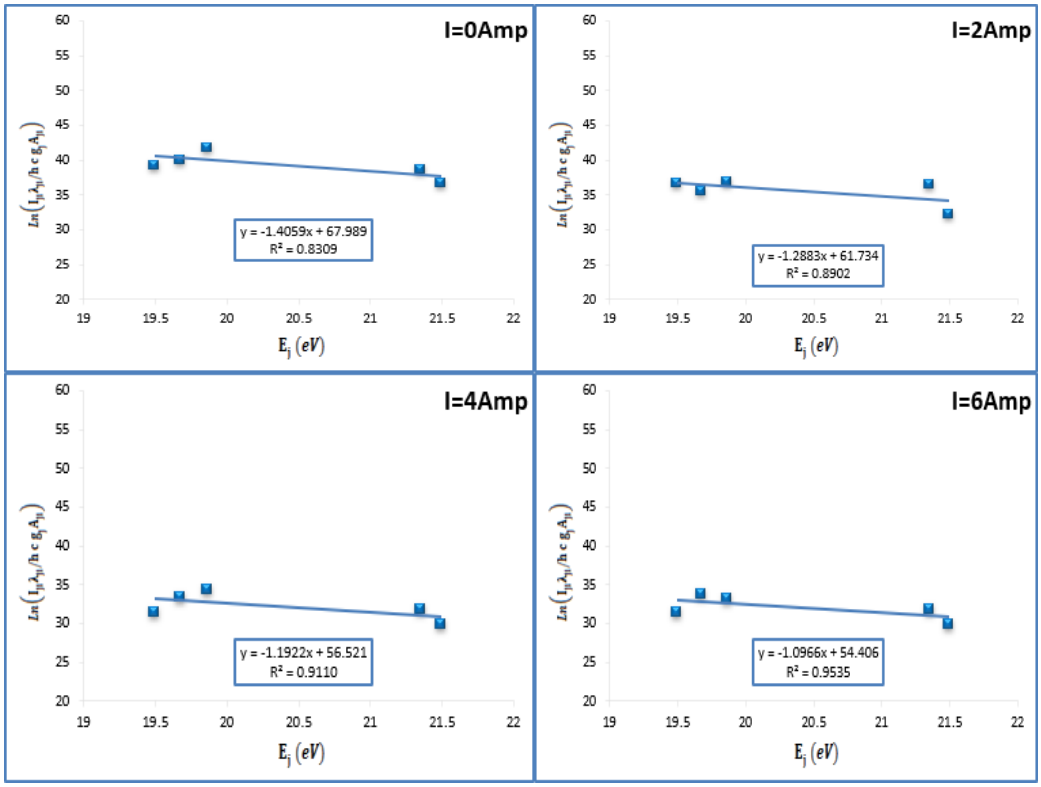

Figure 8: Boltzmann plots for a hollow-discharge configuration with chosen ionic argon lines (Arll) at different coil currents and a source frequency of 9 kHz.

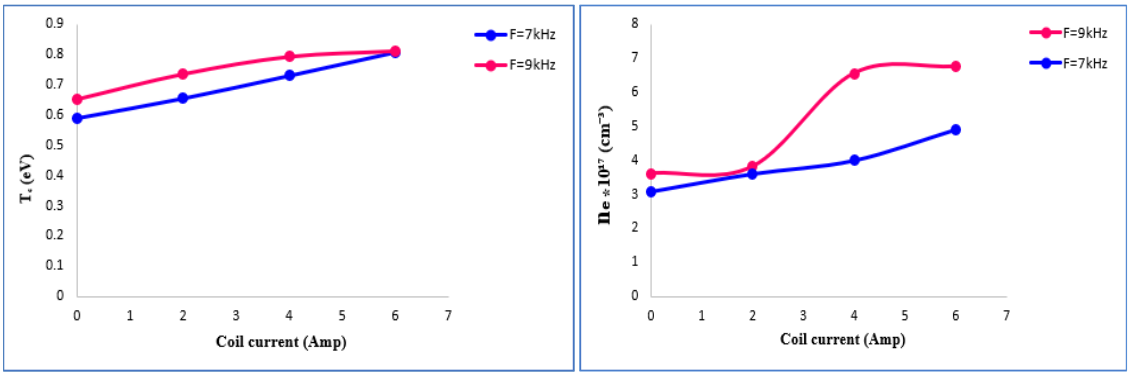

Figure 9: Effect of A.C. frequency on electron temperature and electron number density with the increase of coil current in a hollow cylindrical magnetron sputtering.

Another fundamental discharge parameter calculated in this paper is Debye length (calculated using Eq. 3). Fig. 10 shows how the coil current at the two A.C. frequencies changed the Debye length. It can be seen from this figure that the Debye length decreased with the increase of the coil current. This result means that the sheath surrounding the powered electrode was reduced with the increase of the coil current. This effect increases the volume of plasma. Due to confinement, plasma volume decreases due to the magnetic field.

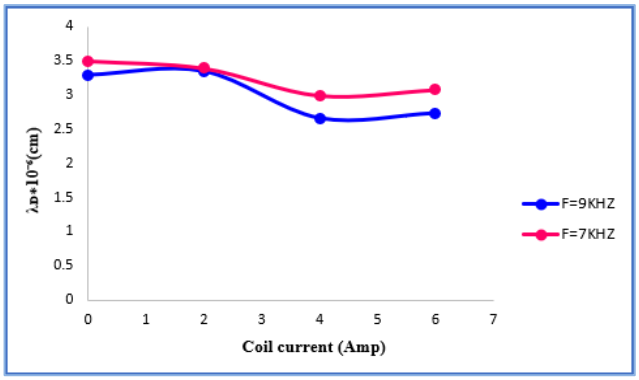

Figure 10: The difference of λD the gas constant pressure with and without B.

Table 2 lists the electron density and Debye length values for the different coil current values for the two source frequencies.

N_D was calculated according to data listed in Table 2 using Eq. 4. The values of N_D for the different coil currents at the two A.C. source frequencies are tabulated in Table 2. The increase in number of the charge particles with the increase of coil current was a result of the increase of ionization collisions. Furthermore, increasing the A.C. frequency from 7 to 9 kHz causes the production of more charge particles due to the increase of the absorbed energy by the electrons.

Table2: The effect of alternating current frequency on discharge parameters at various coil currents.

Plasma Parameter	**Debey length $\times 10^{-6}(cm)$**	**Electron Number Density$\times 10^{17}$ (cm^{-3})**	**Electron Temperature (eV)**	**Coil Current (A)**
		7 kHz		
5569	3.500	3.088	0.685	0
5927	3.393	3.608	0.752	2
5521	2.990	4.912	0.795	4
5989	3.074	4.902	0.839	6
		9 kHz		
5439	3.295	3.615	0.711	0
6037	3.351	3.814	0.776	2
5174	2.658	6.553	0.838	4
5779	2.731	6.749	0.911	6

5. Conclusions

In this study, it was demonstrated that the plasma was subjected to an A.C. discharge. In this investigation, the effects of a magnetic field on plasma properties have been illustrated. It is thought that analyzing the shape of spectral lines is a reliable and non-disturbing way to find out about the properties of argon pressure glow discharge plasma that is made by low-frequency A.C. discharges that run between 7 and 9 kHz. The A.C. discharge plasma properties were measured in magnetron-sputtering plasma using electrodes. The results show the changes in plasma properties as a function of RF power. Additionally, the increase in plasma confinement with a magnetic field results in higher (T_e), (n_e), and (λ_D) than in the absence of a magnetic field.

Acknowledgements

The authors want to express their gratitude and sincere thanks to the Plasma Laboratory in the Physics Department of the College of Sciences, Baghdad University.

Conflict of interest

Authors would like to declare that they do not have any conflict of interests.

References

1. A. Palmero, N. Tomozeiu, A. M. Vredenberg, W. Arnoldbik, and F. Habraken, Surf. Coat. Tech. **177**, 215 (2004).
2. J. Musil and J. Vlček, Mat. Chem. Phys. **54**, 116 (1998).
3. M. Benda and J. Musil, Vacuum **55**, 171 (1999).
4. G. Bleykher, V. Krivobokov, A. Yurjeva, and I. Sadykova, Vacuum **124**, 11 (2016).
5. S. D. Ekpe, F. J. Jimenez, D. J. Field, M. J. Davis, and S. K. Dew, J. Vacu. Sci. Tech. A **27**, 1275 (2009).
6. M. Hassouba, Eur. Phys. J. Appl. Phys. **14**, 131 (2001).
7. N. Tomozeiu, E. Van Faassen, A. Palmero, W. Arnoldbik, A. Vredenberg, and F. Habraken, Thin Sol. Fil. **447**, 306 (2004).
8. Y. Huttel, *Gas-Phase Synthesis of Nanoparticles* (Weinheim, Germany, John Wiley & Sons, 2017).
9. J. P. Squire, C. S. Olsen, F. Chang Díaz, L. D. Cassady, B. W. Longmier, M. G. Ballenger, M. D. Carter, T. W. Glover, G. E. Mccaskill, and E. Bering Iii, 32nd International Electric Propulsion Conference (Wiesbaden, Germany IEPC, 2011). p. 11.
10. X. Ma, T. Furukawa, Y. Oshio, and H. Nishida, AIAA Propulsion and Energy 2020 Forum (Japan ARC, 2020). p. 3629.
11. P. Kelly, P. Henderson, R. Arnell, G. Roche, and D. Carter, J. Vac. Sci. Tech. A: Vac. Sur. Fil. **18**, 2890 (2000).
12. M. Åstrand, T. Selinder, F. Fietzke, and H. Klostermann, Sur. Coat. Tech. **188**, 186 (2004).
13. A. K. Bard and Q. A. Abbas, Optik **272**, 170346 (2023).
14. M. M. Kadhim and Q. A. Abbas, Iraqi J. Sci. **63**, 4254 (2022).
15. N. Idris, T. Usmawanda, K. Lahna, and M. Ramli, Journal of Physics: Conference Series (Medan, Indonesia IOP Publishing, 2018). p. 012098.
16. Q. A. Abbas, A. F. Ahmed, and F. a.-H. Mutlak, Optik **242**, 167260 (2021).
17. M. M. Shehab and K. A. Aadim, Iraqi J. Sci. **62**, 2948 (2021).
18. H. Akatsuka, Advan. Phys. X **4**, 1592707 (2019).
19. H. R. Humud, Iraqi J. Phys. **15**, 142 (2017).
20. U. S. Inan and M. Gołkowski, *Principles of Plasma Physics for Engineers and Scientists* (Cambridge, UK, Cambridge University Press, 2010).
21. I. K. Abbas and K. A. Aadim, Iraqi J. Sci. **64**, 2271 (2023).
22. M. M. Kadhim and Q. A. Abbas, AIP Conference Proceedings (Dubai, United Arab Emirates AIP Publishing, 2021). p. 130024.
23. S. Waheed, S. Bashir, A. Dawood, S. Anjum, M. Akram, A. Hayat, S. Amin, and A. Zaheer, Optik **140**, 536 (2017).
24. S. M. Fathi and S. J. Kadhim, Iraqi J. Sci. **63**, 163 (2022).
25. N. K. Hussein and S. Kadhem, Iraqi J. Sci. **63**, 2492 (2022).
26. Q. A. Abbas, Iraqi J. Phys. **17**, 59 (2019).
27. M. J. Ketan and K. A. Aadim, Iraqi J. Sci. **64**, 188 (2023).

28. A. F. Ahmed and A. A. Yousef, Iraqi J. Sci. **62**, 3560 (2021).
29. Q. A. Abbas, Iraqi J. Sci. **62**, 4694 (2021).
30. M. Fikry, W. Tawfik, and M. M. Omar, Optic. Quant. Elect. **52**, 1 (2020).
31. S. F. Khaleel and Q. A. Abbas, Iraqi J. Sci. **63**, 2470 (2022).
32. R. N. Muhsin and K. A. Aadim, Iraqi J. Phys. **17**, 96 (2019).
33. S. E. Abdulghani and Q. A. Abbas, Iraqi J. Sci. **63**, 2945 (2022).
34. A. K. Bard and Q. A. Abbas, Iraqi J. Sci. **63**, 3412 (2022).
35. A. K. Abbas, K. A. Aadim, and M. F. Jawaad, AIP Conference Proceedings (Dubai, United Arab Emirates AIP Publishing, 2021). p. 080013.
36. H. I. Hussein and K. A. Aadim, Iraqi J. Sci. **63**, 971 (2022).
37. M. A. Essa and K. A. Aadim, Iraqi J. Phys. **17**, 125 (2019).
38. R. K. Hassan, M. A. Aswad, and R. K. Hassan, Indian J. Nat. Sci. **10**, 17908 (2019).
39. I. K. Abbas, Sci. Tech. Indonesia **7**, 508 (2022).
40. K. A. Aadim, Iraqi J. Phys. **15**, 65 (2017).
41. A. Alberti, A. Munafò, M. Koll, M. Nishihara, C. Pantano, J. B. Freund, G. S. Elliott, and M. Panesi, J. Phys. D: Appl. Phys. **53**, 025201 (2019).
42. K. A. Aadim, A. A. Hussain, and W. I. Yaseen, Iraqi J. Phys. **13**, 76 (2015).
43. A. K. Bard and Q. A. Abbas, Indian J. Nat. Sci. **10**, 17908 (2022).
44. A. F. Ahmed, M. R. Abdulameer, M. M. Kadhim, and F. a.-H. Mutlak, Optik **249**, 168260 (2022).
45. M. B. Paul, *Fundamentals of Plasma Physics* (Cambridge, U.K., New York, Cambridge University Press, 2006).
46. M. M. Kadhim, T. H. Khalaf, and Q. A. Abbas, Iraqi J. Sci. **63**, 4771 (2022).
47. R. S. Mohammed, K. A. Aadim, and K. A. Ahmed, Iraqi J. Sci. **63**, 3711 (2022).
48. M. A. Khalaf, B. M. Ahmed, and K. A. Aadim, Iraqi J. Sci. **61**, 1665 (2020).
49. K. A. Aadim, Iraqi J. Phys. **16**, 1 (2018).
50. M. A. Mohammed, H. N. Hashim, and K. A. Aadim, J. Opt., (2023).
51. K. B. Alaa and A. A. Qusay, European Schol. J. **3**, 1 (2022).
52. A. Kramida, Y. Ralchenko, and J. Reader. *NIST Atomic Spectra Database (version 5.10)*; https://www.nist.gov/pml/atomic-spectra-database.

تأثير تردد التيار المتناوب على معلمات التفريغ الترذيذ المغناطيسي المجوف

زهراء محمد حسن[1] وقصي عدنان عباس[1]

[1]قسم الفيزياء، كلية العلوم، جامعة بغداد، بغداد، العراق

الخلاصة

في هذا العمل تم استخدام التحليل الانبعاث البصري لدراسة تأثير تردد مجهز القدرة المتناوب على معلمات الترذيذ المغناطيسي المجوف (انبعاث التفريغ تيار وفولتية التفريغ، درجة حرارة وكثافة العددية للإلكترونات، طول ديباي معلم بلازما) عند ضغط ثابت. تم حساب درجة حرارة وكثافة العددية للإلكترونات باستخدام طريقة بولتزمان وكذلك توسع ستارك. حيث بينت النتائج ان تركيب التوهج الطبيعي يشبه التركيب في حالة التفريغ المستمر. وان تأثير مجال مغناطيسي على تركيب التفريغ يكون مشابه لسلوك التيار المستمر. كما لوحظ ان مجال مغناطيسي لا يمتلك تأثير على معلمات الأساسية للتفريغ في كلا الترددي المصدر المتناوب من ناحية أخرى فان بقية معلمات التفريغ (درجة حرارة الالكترون، الكثافة العددية للإلكترون، طول ديباي عدد جسيمات في كرة ديباي) تزداد بزيادة مجال المغناطيسي في كلا الترددين بالإضافة الى ذلك فان زيادة تردد مصدر المتناوب ادى الى زيادة شدة الانبعاث وكذلك بقية معلمات البلازما التي تم دراستها.

الكلمات المفتاحية: القطب المجوف، درجة حرارة الالكترون، تفريغ التيار المتناوب، الكثافة العددية للإلكترونات، تيار التفريغ.